



The development of low-temperature heat-treatable high-pressure die-cast Al–Mg–Fe–Mn alloys with Zn

Xiangzhen Zhu¹, Fuchu Liu^{1,2,3}, Shihao Wang¹, and Shouxun Ji^{1,*}

¹ Brunel Centre for Advanced Solidification Technology (BCAST), Brunel University London, Uxbridge Middlesex UB8 3PH, UK

² School of Mechanical Engineering and Electronic Information, China University of Geosciences, Wuhan 430074, China

³ State Key Laboratory of Materials Processing and Die & Mould Technology, Huazhong University of Science and Technology, Wuhan 430074, China

Received: 14 October 2020

Accepted: 25 February 2021

Published online:

18 March 2021

© The Author(s) 2021

ABSTRACT

In the present work, a novel low-temperature heat-treatable recycled die-cast Al–Mg alloy was developed by adding Zn into non-heat-treatable Al–5Mg–1.5Fe–0.5Mn alloy. The results showed that Zn additions resulted in the formation of equilibrium phase T-Mg₃₂(Al, Zn)₄₉ under as-cast condition, which can be dissolved into the α -Al matrix at a relatively low solution temperature (430 °C) and thus set the base for the low-temperature heat treatment. The mechanical test results indicated that Zn additions had a smooth liner improvement in the strength of all as-cast alloys and T6-state alloys with 1% and 2% Zn as its concentration increased but resulted in a sharp improvement on the strength of T6-state alloy when Zn concentration increased from 2 to 3%. TEM analysis revealed that the precipitate in T6-state Al–5Mg–1.5Fe–0.5Mn–3Zn alloy is η' phase, rather than the widely reported T'' or T' phase in other Al–Mg–Zn alloys with approximately same Mg and Zn concentrations. After the optimized low-temperature T6 heat treatment (solution at 430 °C for 60 min and ageing at 120 °C for 16 h), the Al–5Mg–1.5Fe–0.5Mn–3Zn alloy exhibits the yield strength of 321 MPa, ultimate tensile strength of 445 MPa and elongation of 6.2%.

Handling Editor: P. Nash.

Xiangzhen Zhu and Fuchu Liu contributed equally to this work.

Address correspondence to E-mail: shouxun.ji@brunel.ac.uk

<https://doi.org/10.1007/s10853-021-05972-5>

Introduction

Al–Mg-based alloys are typical lightweight structural materials and are characterized by non-heat treatable, higher strength and ductility under as-cast condition in comparison with Al–Si-based alloys [1, 2]. With the significantly technological progress in recent years in aerospace and automobile industry and the increased requirements in materials recycling for energetic and environmental benefits [3, 4], the improvement in mechanical properties of lightweight components is always in great demand. For cast Al–Mg-based alloys, one of the effective approaches to increase their strength and ductility is to add effective elements into conventional non-heat-treatable alloys and apply heat treatment for precipitate strengthening. The two most popular improved Al–Mg alloys are Al–Mg–Zn [4–6] and Al–Mg–Cu–Zn [7, 8], in which $T\text{-Mg}_{32}(\text{Al}, \text{Zn})_{49}$ and $S\text{-Al}_2\text{MgCu}$ phases and their precursors were formed and largely improve the mechanical properties. Meanwhile, Si is also added into Al–Mg alloys to form the strengthening Mg_2Si phase and its precursors in Al–Mg–Si–Zn [9–11] and Al–Mg–Si–Cu–Zn [12–14].

High-pressure die casting (HPDC) is a popular method for producing structural components in automotive industry due to its large advantages in high productivity, good dimensional accuracy and capacity of making complex and thin-wall castings [15]. With the significant progress of HPDC technology derived by increased requirements in the past decades, the development and application of new alloys with excellent properties are considered as an important way to offer high-quality castings [16]. Recently, a high-strength Al–Mg–Fe–Mn alloy was developed for high-pressure die casting [17, 18], achieving the ultimate tensile strength of > 300 MPa, the yield strength of about > 150 MPa and the tensile elongation of $> 10\%$ under as-cast condition. Moreover, the application of conventional detrimental Fe and Mn elements to form intermetallic for strengthening can successfully increase the yield strength of alloys. However, this new Al alloy currently is non-heat treatable and thus cannot be further strengthened by using solution and ageing heat treatment. It is attractive to improve its microstructure and mechanical properties by adding a suitable addition. Considering the presence of iron (1.5 wt%) and manganese (0.5 wt%), Si is not suitable to strengthen

this Al–Mg–Fe–Mn alloy because it would largely increase the volume of Fe-bearing intermetallics and thus decrease the elongation quite significantly. Compared with Cu, Zn is a cost-effective addition into Al–Mg alloys to improve the strength. Moreover, it was also reported that the Zn addition in the Al–Mg alloy can enhance the intergranular corrosion resistance of Al–Mg alloys [19].

But, except the advantages of HPDC technology, it also brings a shortage of die castings. Due to the turbulence of melt during die-filling process, die castings usually contain too much trapped gas. Heat treatment, especially the solution treatment at a high temperature, would make the impressed trapped gas expand greatly to form surficial blisters and inside big porosities, resulting in poor and scattered mechanical properties [1]. Therefore, the feature of solutionizing at relatively low temperature and the subsequently precipitation process are very important for the thin-wall castings made by high-pressure die casting because much less blisters, residual stress and distortion in components will be possible through lowering the solution temperature. The literature reported a series of solution temperatures for wrought Al–Mg–Zn alloys including 530 °C [8], 495 °C [20], 470 °C [21] and even 465 °C [22, 23]. It is not mentioned whether these solution treatments are complete solutions or just partial solutions. However, it indicates that a low-temperature (such as 465 °C) solution treatment is possible for die-cast Al–Mg–Fe–Mn–sZn alloys.

Therefore, in the present work, it is aimed to investigate the effects of Zn levels on the microstructure and mechanical properties of Al–5Mg–1.5Fe–0.5Mn alloys processed by high-pressure die casting under as-cast and heat-treated conditions. The heat treatment was studied and optimized at relatively low temperature, and the related precipitates were identified by TEM. Meanwhile, the phase formation in as-cast alloy was also analysed through the calculation of phase diagrams (CALPHAD) modelling of multicomponent Al–Mg–Fe–Mn–Zn system. The relationship between solidification path, microstructure, mechanical properties and the strengthening mechanisms was also discussed.

Experimental process

Commercially pure Al, Mg and Zn, Al–45Fe and Al–20Mn master alloy ingots (all compositions quoted in this paper are in wt% unless otherwise stated) were used to prepare the alloys with a nominal composition of Al–5Mg–1.5Fe–0.5Mn (hereafter denoted AlMgFeMn) with different Zn levels. During experimental preparation, each element was weighted to a calculated ratio with additional amounts for compensating the burning loss during melting. The melting was carried out in a 12-kg clay–graphite crucible coated with boron nitride using an electric resistance furnace at 780 ± 5 °C. The ingots including Al, Fe and Mn elements were loaded into the crucible and melted first. Zn and Mg ingots which had been preheated to 200 °C were then carefully added into the completely molten alloy. After one hour of homogenization at 750 °C, the melt was degassed using high-purity argon through a rotary impeller at a speed of 300 rpm for 5 min, resulting in the density index $< 2\%$.

After degassing, the melt was covered by a commercial granular flux (Coveral GR 6512, Foseco, UK), and then, the furnace was maintained at 750 °C for 20 min for temperature recovery. The $\Phi 40 \times 60$ mm cylindrical samples for composition analysis were obtained by pouring the melt into a permanent steel mould preheated at 200 °C. The cylindrical samples were cut across the diameter at 20 mm from the bottom before applying the composition analysis. The chemical compositions were measured using a well-calibrated optical emission spectrometer (OES, Foundry-Master Pro, Oxford Instrument Ltd., UK) with testing at least five sparks, and the average value was taken as the actual chemical composition of the alloys, as listed in Table 1.

After composition analysis and skimming, the melt was manually dosed and subsequently loaded into the shot sleeve of a 4500 kN cold-chamber HPDC machine (Frech DAK 450–54, Germany) under the optimized control condition, in which all casting parameters were digitally set and controlled. The

casting die block was heated and maintained at 150 °C by the circulation of mineral oil, and the shot sleeve was heated and maintained at 90 °C by the circulation of pressurized hot water. The pouring temperature of melt was 730 °C measured by a K-type thermocouple. Eight ASTM B557M standard round tensile testing bars with a gauge dimension of $\Phi 6.35 \text{ mm} \times 50 \text{ mm}$ were cast in each shot. All casting samples were kept at ambient condition for three days before heat treatment and tensile testing.

Heat treatment was performed in an air-circulated electric resistance furnace, which was preheated to a pre-set temperature and maintained this temperature for 1 h before putting the samples into the chamber of the furnace. The temperature inside the furnace chamber was measured by a separate K-type thermocouple, which manifested the temperature deviation of ± 0.5 °C during all the heat treatment experiments. Solution treatment was performed at 430 °C and 490 °C for different times, followed by an immediate water quenching using cold water. Ageing treatment was carried out at 120 °C and 180 °C for different times, followed by air cooling to ambient temperature.

Tensile testing was conducted according to ASTM standard B557M and ASTM E8/E8M-16 Standard Test Methods for Tension Testing of Metallic Materials (Instron 5500 Universal Electromechanical Testing Systems equipped with Bluehill software) and a ± 50 kN load cell. The elongation of samples was evaluated using an extensometer with a gauge length of 50 mm, and the ramp rate was controlled as 1 mm/min during tensile tests. At least seven samples without showing obvious defects on the fractured surface were measured to obtain the average value of ultimate tensile strength (UTS), yield strength (YS) and elongation (EI). Vickers hardness testing (Wilson 432 SVD digital auto turret Vickers Hardness Tester) was performed on the polished samples with a load of 5 kg and a dwell time of 10 s. Ten measurements were conducted in individual sample, and the average was taken as reported

Table 1 Chemical compositions of experimental alloys analysed by OES (wt%)

Alloy	Mg	Fe	Mn	Zn	Si	Others	Al
AlMgFeMn	5.06 ± 0.08	1.54 ± 0.11	0.51 ± 0.05	Varied*	0.04 ± 0.01	< 0.04	Bal

* Actual Zn levels were measured to be 0.02 ± 0.06 , 1.07 ± 0.06 , 2.07 ± 0.05 and 3.09 ± 0.06 , respectively

hardness. All tensile and hardness tests were performed at ambient temperature ($\sim 20\text{ }^{\circ}\text{C}$).

The X-ray diffraction (XRD) patterns of the samples were carried out using the D8 Advance X-ray diffractometer equipped with Cu $K\alpha$ radiation in the range of 20° – 90° at a scanning speed of $1^{\circ}/\text{min}$. The specimens for microstructural characterization were taken from the middle of $\Phi 6.35$ -mm round tensile bars and then mounted, mechanically grounded and polished. In order to observe 3D morphologies of the Fe-rich intermetallic phase in the experimental alloys, a 15 vol% HCl–distilled water solution was used to deep-etch or completely remove the matrix of the specimens. The Keller agent (1 vol% HF, 1.5 vol% HCl, 2.5 vol% HNO_3 and 95 vol% H_2O) was used for chemical etching. The microstructure was examined utilizing a Zeiss optical microscope (OM), a Zeiss SUPRA 35VP field emission scanning electron microscope (SEM) equipped with energy-dispersive X-ray spectroscopy (EDS) and electron backscattered diffraction (EBSD) working at an accelerating voltage of 20 kV and a JEOL-2100 transmission electron microscope (TEM) operating at an accelerating voltage of 200 kV. To prepare thin foils for TEM examination, slices of HPDC samples were mechanically ground and punched into 3-mm-diameter discs. These discs were manually ground to approximately $100\text{ }\mu\text{m}$ in thickness followed by twin-jet electron-polishing at 15 V and $-25\text{ }^{\circ}\text{C}$ using a solution of 30% nitric acid in methanol. The quantitative EDS analysis in SEM was conducted at a 20 kV accelerating voltage on the polished specimens. To minimize the influence from the interaction volume during EDS quantification, at least five-point analysis on selected particles or areas was carried out for each phase and the average was taken as the measurement. To measure the volume fraction of intermetallic phases in the alloys, SEM images were taken from at least three random locations of each alloy at a magnification of $1000\times$ and then analysed by using the quantitative image analysis software ImageJ. The average size of α -Al grains was calculated by the software TSL OIM analysis according to the tested EBSD inverse pole figure (IPF) map.

Experimental results

As-cast microstructure and mechanical properties

Figure 1 shows the XRD spectrums of the as-cast AlMgFeMn alloys with different Zn levels. It indicates that α -Al and $\text{Al}_6(\text{Fe}, \text{Mn})$ always existed in all alloys. Meanwhile, the peak of $\text{T-Mg}_{32}(\text{Al}, \text{Zn})_{49}$ phase was also observed in the alloy with Zn additions, and its strength was increased as Zn levels were increased. Figure 2 is the EBSD inverse pole figure (IPF) map showing α -Al grain size of AlMgFeMn alloys without and with 3wt% Zn. The results show that all alloys have very fine α -Al grains with an average size of $10 \pm 3.1\text{ }\mu\text{m}$ and no significant difference was found in the size and morphologies of the primary α -Al phase in the experimental AlMgFeMn alloys with different levels of Zn. It was also found that the size of α -Al grains showed a bi-model distribution. Most α -Al grains were fine globular particles with a size of less than $20\text{ }\mu\text{m}$ (marked as α -Al₁), while there also existed a few large dendritic and fragmented dendritic α -Al grains ranging from 20 to $100\text{ }\mu\text{m}$. The coarsened α -Al grains were isolated by fine globular α -Al grains (marked as α -Al₂). The formation of these two kinds of α -Al grains was induced by the two-step solidification during cold-chamber HPDC process [24].

Figure 3 shows the effect of Zn levels on the as-cast microstructure of AlMgFeMn alloys. The lath-like or rhombic bright white phase was Fe rich and showed atomic ratio of Al to Fe/Mn of about 6. This phase

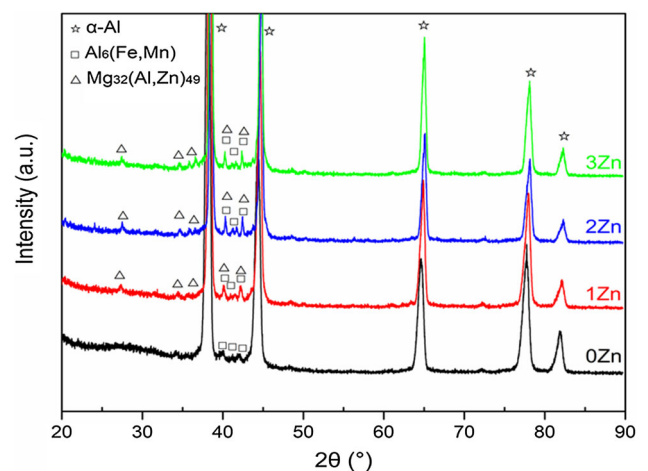


Figure 1 XRD spectrums of the AlMgFeMn alloys with different Zn levels under as-cast condition.

Figure 2 EBSD inverse pole figure (IPF) map showing α -Al grain size of AlMgFeMn alloys **a** without and **b** with 3.09Zn.

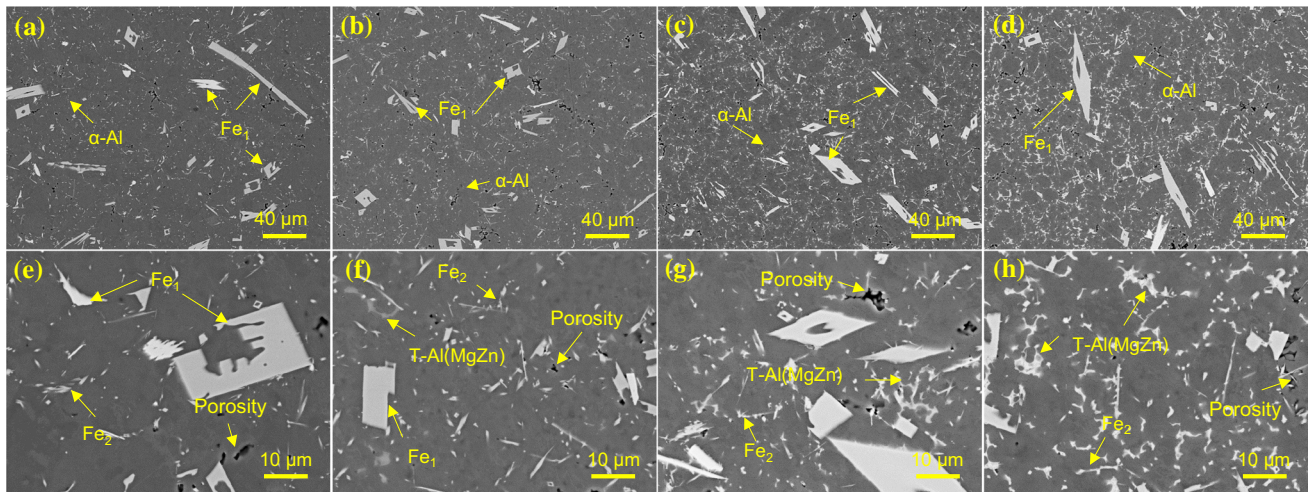
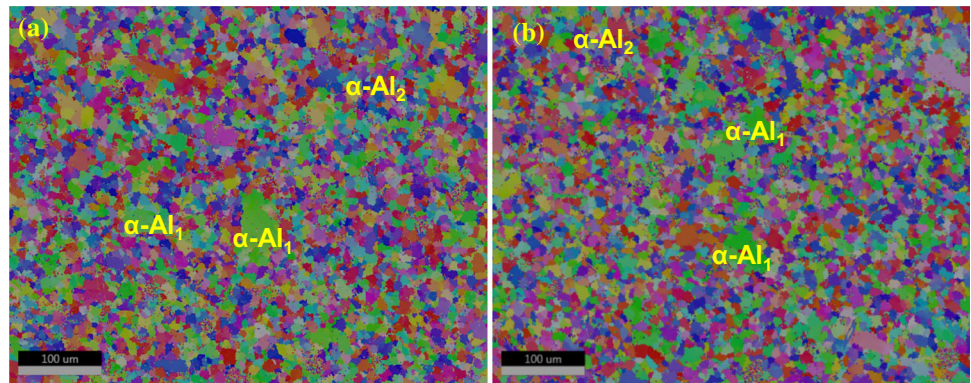


Figure 3 Backscattered SEM images showing the as-cast microstructure of AlMgFeMn alloys with **a, e** 0.02Zn, **b, f** 1.07Zn, **c, g** 2.07Zn and **d, h** 3.09Zn.

was identified as $\text{Al}_6(\text{Fe}, \text{Mn})$ phase. It is also seen that $\text{Al}_6(\text{Fe}, \text{Mn})$ particles also had a bi-model distribution in size and were labelled as Fe_1 and Fe_2 in Fig. 3. This phenomenon is in consistent with the result observed in Al–Mg alloys in our previous study [17, 24]. The other irregular bright white phase along α -Al grain boundaries was found to be Mg rich and Zn rich and can be identified as $\text{T-Mg}_{32}(\text{Al}, \text{Zn})_{49}$ phase from the XRD information. From Fig. 3, it is clear that the amount of $\text{T-Mg}_{32}(\text{Al}, \text{Zn})_{49}$ phase was steadily increased in the alloys with higher Zn levels. No other Mg-rich or Zn-rich intermetallics were found. From the composition analysis of α -Al and $\text{T-Mg}_{32}(\text{Al}, \text{Zn})_{49}$ phases shown in Table 2, it is interesting to note that the primary α -Al phase contained 5.55% Mg in the alloy without Zn, meaning that all Mg atoms were dissolved into the Al matrix in the alloy without Zn. When Zn was added into the alloys, the concentration of Mg dissolved in α -Al grains was reduced to 3.63%, 3.38% and 3.18%

gradually; meanwhile, more Zn atoms were also dissolved in α -Al grain and its level was increased to 0.38%, 1.07% and 1.76%, respectively. Moreover, the atomic ratio of Mg to Zn in $\text{T-Mg}_{32}(\text{Al}, \text{Zn})_{49}$ phase was also decreased as more Zn atoms were added into the experimental alloys.

From Figure 3, it is known that primary $\text{Al}_6(\text{Fe}, \text{Mn})$ particles were presented in the shape of rhomboid or lath in 2D section, and most rhomboid had an internal hollow. To further reveal the morphology of $\text{Al}_6(\text{Fe}, \text{Mn})$ particles, they were extracted from the alloys by removing Al matrix using HCl solution. Figure 4 shows its typical 3D morphology. Clearly, the primary $\text{Al}_6(\text{Fe}, \text{Mn})$ crystals showed a prism shape with an inside hollow in all alloys with or without Zn. It can be concluded that both rhombic and lath-like 2D morphologies shown in Figure 3 are the crossed sections in prism shapes.

Figure 5 displays the mechanical properties of as-cast AlMgFeMn alloys with different Zn levels

Table 2 Quantitative analysis of the phases in the AlMgFeMn alloys with different Zn levels under as-cast condition

Zn content in alloy (wt%)	Phase	Phase composition (wt%)				
		Al	Mg	Fe	Mn	Zn
0.02	α -Al	94.45 \pm 3.69	5.55 \pm 1.02	0	0	0
	α -Al	95.99 \pm 3.23	3.63 \pm 0.89	0	0	0.38 \pm 0.10
1.07	AlMgZn	83.27 \pm 4.51	10.88 \pm 2.64	0	0	5.85 \pm 1.12
	α -Al	95.55 \pm 4.02	3.38 \pm 0.80	0	0	1.07 \pm 0.14
2.07	AlMgZn	72.08 \pm 4.69	13.67 \pm 3.20	0	0	14.25 \pm 2.95
	α -Al	95.06 \pm 6.23	3.18 \pm 0.75	0	0	1.76 \pm 0.22
3.09	AlMgZn	54.7 \pm 4.69	21.3 \pm 3.95	0	0	24 \pm 4.49

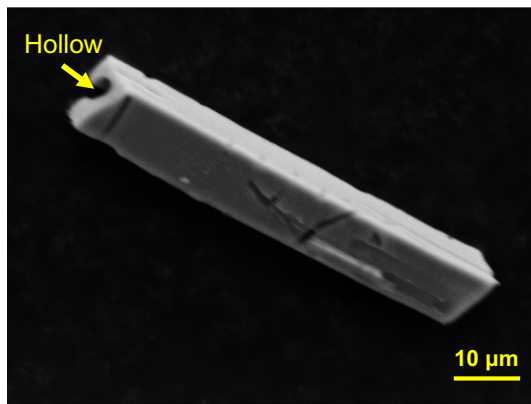


Figure 4 SEM micrograph showing the 3D morphology (longitudinal direction) of the primary $Al_6(Fe, Mn)$ phase in AlMgFeMn alloys with different Zn levels.

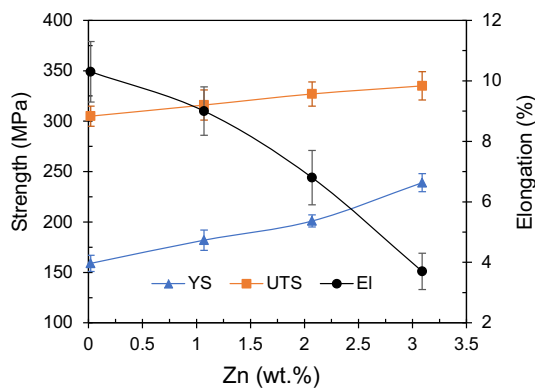


Figure 5 The effect of Zn levels on the mechanical properties of as-cast AlMgFeMn alloys at room temperature.

measured at room temperature. It is seen that the increase in Zn levels from 0.02 to 3.09% resulted in a linear improvement in the ultimate tensile strength from 305 to 335 MPa, yield strength from 159 to 239 MPa, but a significant decrease in the elongation from 10.3 to 3.7%.

T6 heat treatment and its effect on the microstructure and mechanical properties

The addition of Zn leads to the formation of $T-Mg_{32}(Al, Zn)_{49}$ phase under as-cast condition, which has a varying solubility in α -Al matrix as the temperature varies and thus makes the experimental Al-Mg alloys be strengthened by different mechanisms after heat treatment. To reach a higher strength of the experimental alloys, the solution and ageing were investigated, and the corresponding microstructure evolution and mechanical properties were analysed in the present work.

Three temperatures were adopted as solution temperatures for the experimental AlMgFeMn alloys with 3.09Zn. Figure 6 shows the effect of solution temperature and time on the volume fraction of T phase and hardness. It is clear that the alloy showed an apparent decrease in the volume fraction of $T-Mg_{32}(Al, Zn)_{49}$ phase and the hardness with the increase in solution time at different solution temperatures. The hardness reached a similar stable value of 85 HV. It was also noticed that the higher temperature 490 °C could shorten the solution process and reduced the solution time from 60 min at 430 °C to 30 min 490 °C. However, considering lower solution temperature would induce less porosities, residual stress and distortion, it is significant to use low solution temperature in practice.

Figure 7 shows the microstructural evolution of AlMgFeMn alloy containing 3.09Zn during the solution treatment at 430 °C. Clearly, the $T-Mg_{32}(Al, Zn)_{49}$ intermetallic phase could be dissolved into the α -Al matrix at 430 °C. After 60 min, the irregular $T-Mg_{32}(Al, Zn)_{49}$ intermetallic phase was disappeared. However, there was no obvious change in the morphology and amount of $Al_6(Fe, Mn)$ phase after

Figure 6 Effect of solution time and temperature on the **a** volume fraction of T-Mg₃₂(Al, Zn)₄₉ phase and **b** hardness of experimental AlMgFeMn alloys with 3.09Zn.

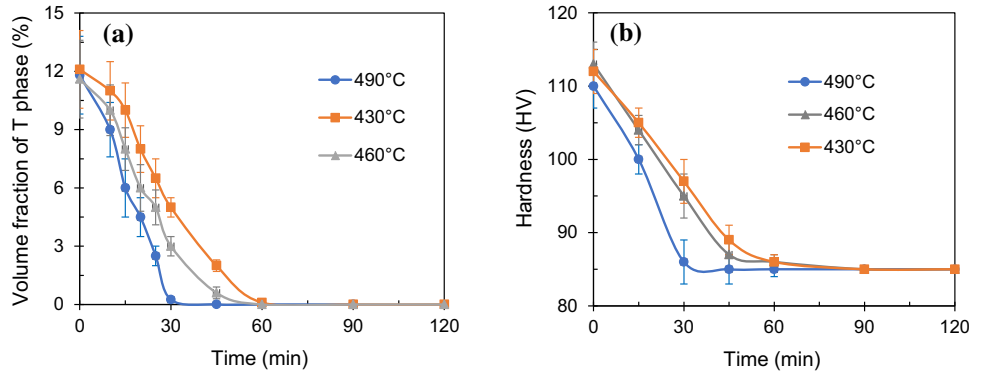
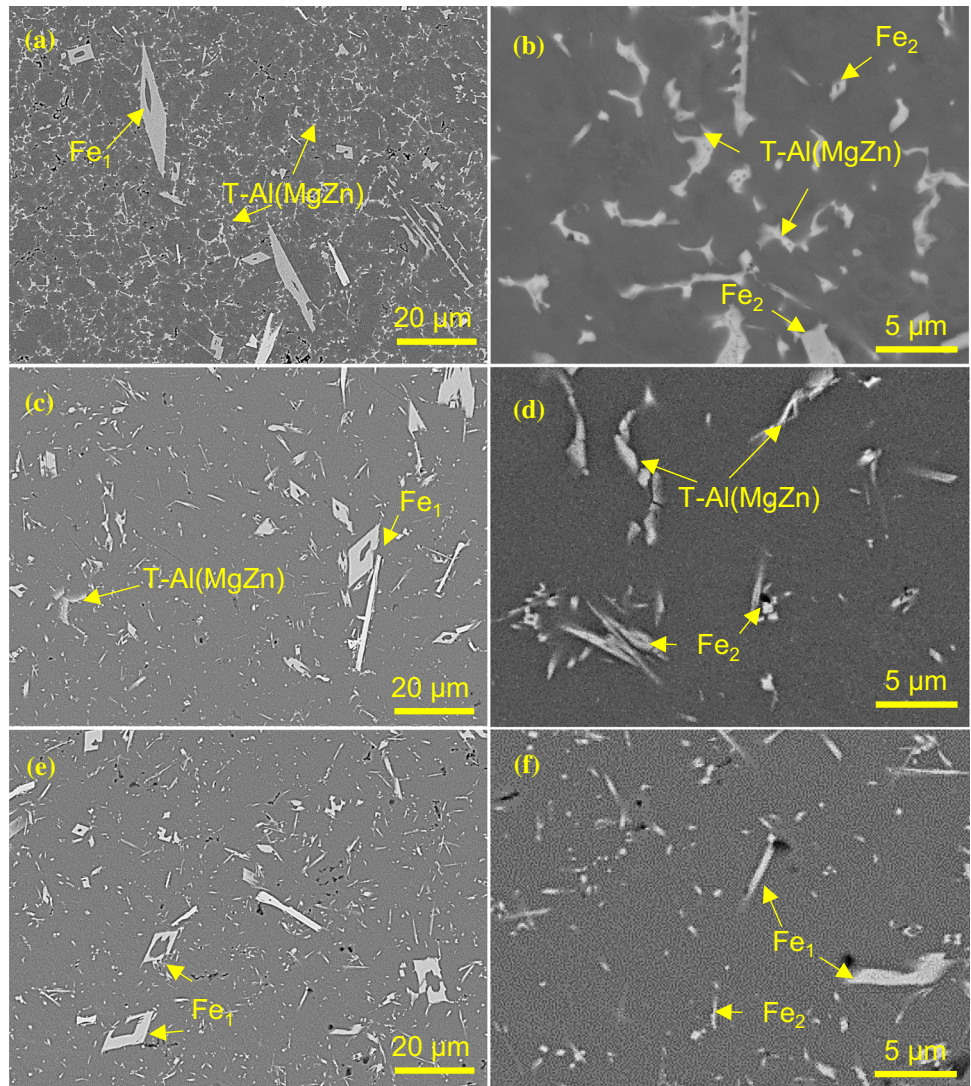


Figure 7 Microstructure of AlMgFeMn alloy with 3.09 Zn after the solution treatment at 430 °C for different times: **a**, **b** 0 min, **c**, **d** 30 min and **e**, **f** 60 min.



solution treatment. The XRD spectra shown in Fig. 8 further confirmed that all experimental alloys with different Zn levels would only contain α -Al and Al₆(Fe, Mn) phases after the solution treatment at 430 °C for 60 min and all T-Mg₃₂(Al, Zn)₄₉ phase

dissolved completely. As the result of the dissolution of T-Mg₃₂(Al, Zn)₄₉ phase, almost all Mg and Zn atoms exist in the form of solute atoms in α -Al matrix, as shown in Table 3.

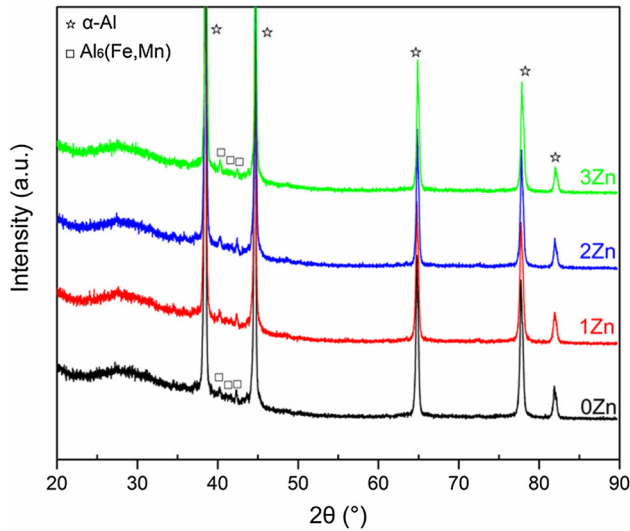


Figure 8 XRD spectra of the AlMgFeMn alloys with different Zn levels after solution treatment at 430 °C for 60 min.

After the complete solution heat treatment, the subsequent ageing heat treatment was carried out for the formation of precipitates to improve the mechanical properties of the alloys. Figure 9a shows the hardness of die-cast Al–Mg–Fe–Mn alloy with 3.09Zn after solution treatment of 430 °C for 60 min and subsequently aged at 120 °C and 180 °C for different times. For the ageing at 180 °C, it is seen that the hardness was increased to the peak of 127 Hv at 2 h, followed by a decrease with prolonged ageing to a stable hardness at about 110 Hv. Similar trend was found for the ageing at 120 °C, but the peak hardness of 136 Hv was obtained at a longer time of 20 h. However, the hardness at 16 h reached 135 Hv, which is very close to the peak hardness at 20 h. Therefore, for the energy saving, the ageing time at 120 °C for following tensile samples was decided as 16 h. It is noticed that the peak-aged time is much shorter than the reported peak-aged time of other similar Al–Mg alloys. Lucas found that a wrought Al–4.7Mg–0.4Mn–3.5Zn alloy aged at 125 °C after a solution heat treated at 465 °C for 35 min with water

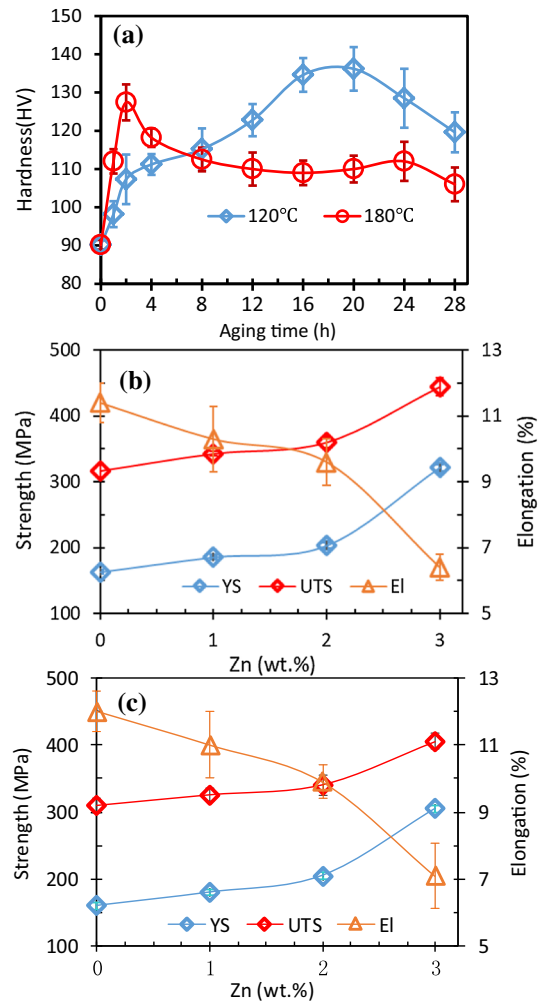


Figure 9 a Effect of ageing time on the hardness of die-cast AlMgFeMn alloy with 3.09Zn after solution treatment of 430 °C for 60 min and subsequently aged at 120 °C and 180 °C, b, c effect of the Zn level on the tensile properties of the AlMgFeMn alloy after solution treatment at 430 °C for 60 min and ageing at b 120 °C for 16 h and c 180 °C for 2 h.

quench needed 9 days to reach its peak hardness [22]. Under a same solution and quenching conditions, Lucas further reported that the peak hardness of an Al–5Mg–0.8Mn–3.8Zn alloy prepared by HPDC was

Table 3 Quantitative analysis of the α -Al phase in the heat-treated AlMgFeMn alloys with different Zn levels

Zn content in alloy (wt%)	α -Al phase composition (wt%)				
	Al	Mg	Fe	Mn	Zn
0.02	94.92 ± 1.86	5.08 ± 0.43	0	0	0
1.07	94.01 ± 1.53	4.97 ± 0.62	0	0	1.02 ± 0.16
2.07	92.89 ± 2.47	5.16 ± 0.82	0	0	1.95 ± 0.23
3.09	91.85 ± 2.76	5.19 ± 0.56	0	0	2.96 ± 0.20

not reached after an ageing time of about 110 h at 125 °C [23].

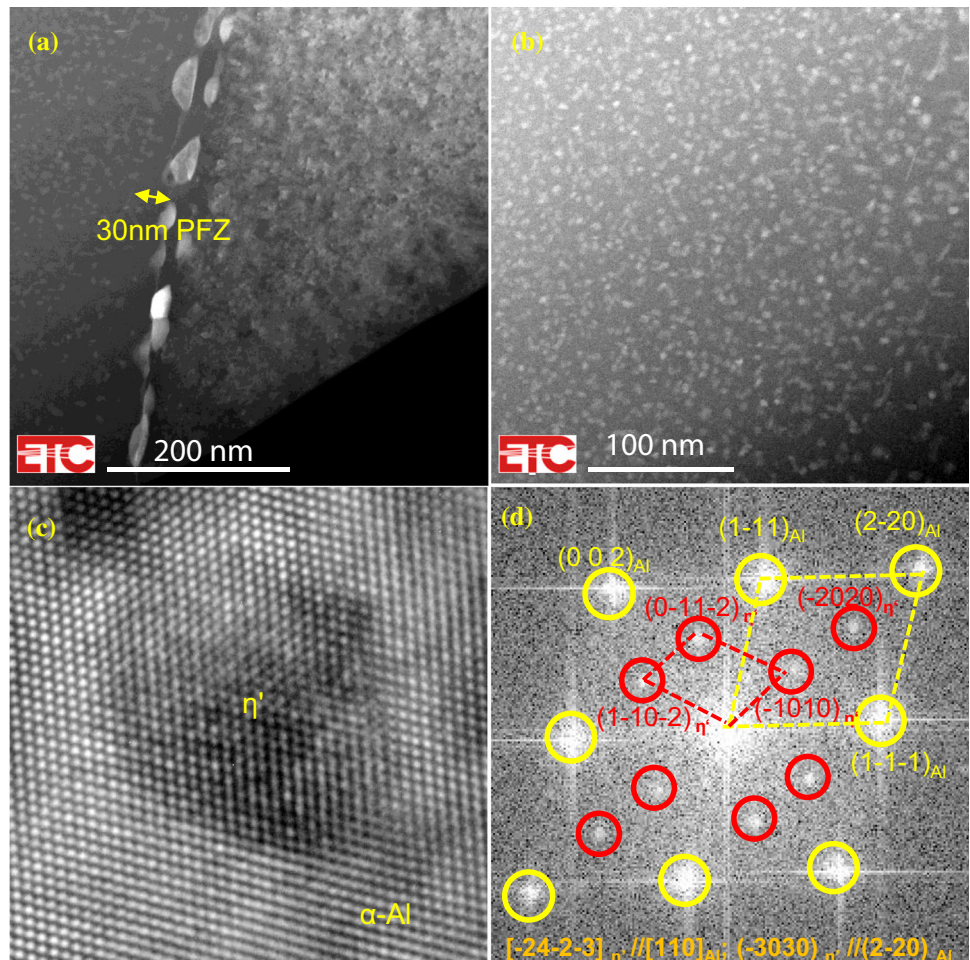
Figure 9b and c shows the mechanical properties of the experimental alloys after solution at 430 °C for 60 min and ageing at 120 °C for 16 h and 180 °C for 2 h, respectively. It is clear that, after T6 heat treatment, the strength of experimental alloys was significantly improved at the sacrifice of elongation. When Zn addition was increased from 0.02 to 3.09% and the ageing temperature was 120 °C, the ultimate tensile strength (UTS) was significantly increased from 316 to 444 MPa and the yield strength (YS) was also significantly increased from 163 to 321 MPa, but the elongation was significantly decreased from 11.4% in the alloy without Zn addition to 6.2% for the alloy with 3.09Zn. The similar trend of mechanical properties was found when the experimental alloys were aged at 180 °C for 2 h. But in this case, both the improvement in strength and the sacrifice of elongation were slightly reduced. An interesting

phenomenon was noticed here. As shown in Fig. 5 and Fig. 9b, c, the addition of Zn showed a good strengthening effect on AlMgFeMn alloys. However, the strength improvement was not alignment in linear trends with the level of Zn addition, especially for the T6-treated alloys. For example, when the ageing time was 120 °C, Zn addition increased from 2.07 to 3.09% could dramatically improve the yield strength of 118 MPa from 203 to 321 MPa and the ultimate tensile strength of 85 MPa from 360 to 445 MPa. As the comparison, the strength improvement induced by the increment of Zn addition from 0 to 1% or 1 to 2% is less than 26 MPa.

Phase identification of precipitate in T6-treated alloy

To understand the strengthening mechanism, TEM observations were performed for the AlMgFeMn alloy with 3.09Zn after the solution at 430 °C for 60 min and subsequently aged at 120 °C for 16 h. The

Figure 10 TEM images showing **a** precipitate free zones (PFZ) along α -Al grain boundary and **b** well-distributed precipitates in α -Al matrix in AlMgFeMn alloy with 3.09Zn after 430 °C solution for 60 min and aged 120 °C for 16 h; **c** HRTEM of a η' precipitate and **d** its corresponding fast Fourier transform (FFT) pattern.



corresponding microstructural characteristics are presented in Fig. 10. Figure 10a indicates that the alloy showed narrow precipitate free zones (PFZ) with the width of approximately 30 nm. As shown in Fig. 10b, numerous dot-like precipitates ranged from 3 to 10 nm and a few rod-like precipitates with a maximum length of 25 nm were uniformly distributed in the α -Al matrix. It should be mentioned that these dot-like precipitates might be the projections of the rod-like precipitates under the different observation direction. Figure 10c, d displays the HRTEM image and corresponding fast Fourier transform (FFT) pattern of a typical precipitate. It is evidently clear that the precipitate was coherent with the Al matrix. According to the FFT pattern shown in Fig. 10d, the precipitate showed several weak diffraction spots located at the $1/3$ and $2/3$ $(2-20)_{\text{Al}}$ positions and was identified as η' phase, rather than the widely reported T'' or T' phase in Al–Mg alloys [7, 8, 19, 20, 25, 26]. The orientation relationships between the η' precipitate and α -Al matrix could be described as $[-24-2-3]_{\eta'} // [110]_{\text{Al}}; (-3030)_{\eta'} // (2-20)_{\text{Al}}$. It was reported that η' phase is a metastable phase with space group $P63/mmc$ [27, 28]. Here, it should be mentioned that, in one of our previous work [28], a diffraction patterns model from η' precipitate with hexagonal crystal structure was established systematically under the $[110]_{\text{Al}}$ zone axis and showed a good agreement with the experimental result. The orientation relationship appeared

in the present work is same with one configuration of this model which has four variants in total.

Discussion

Solidification path and microstructural evolution

The solidification path and microstructural evolution can be understood using the phase diagram of the multicomponent Al–Mg–Fe–Mn–Zn system. The equilibrium phase diagram of Al–Mg–Fe–Mn–Zn system on the cross section of the Al–5Mg–1.5Fe–0.5Mn was calculated by Pandat software and PanAl2018 Thermodynamic database, as shown in Fig. 11a. It is found that $\text{Al}_{13}\text{Fe}_4$ and α -Al phases should precipitate directly from melt, and then $\text{Al}_6(\text{Fe}, \text{Mn})$, β -AlMg or $\text{T-Mg}_{32}(\text{Al}, \text{Zn})_{49}$ phases precipitated via solid reactions. The addition of Zn would promote the formation of $\text{T-Mg}_{32}(\text{Al}, \text{Zn})_{49}$ but suppress the formation of β -AlMg. However, comparing the as-cast microstructures and equilibrium phase diagram, it is clear that the equilibrium $\text{Al}_{13}\text{Fe}_4$ and β -AlMg phases is not formed. Instead, $\text{Al}_6(\text{Fe}, \text{Mn})$ phase is the dominant Fe-rich phase. The differences can be attributed to several factors including the variation of the actual non-equilibrium solidification in HPDC process and the accuracy of the database used in the phase diagram calculation. Our previous results have confirmed that the Mn atoms played a

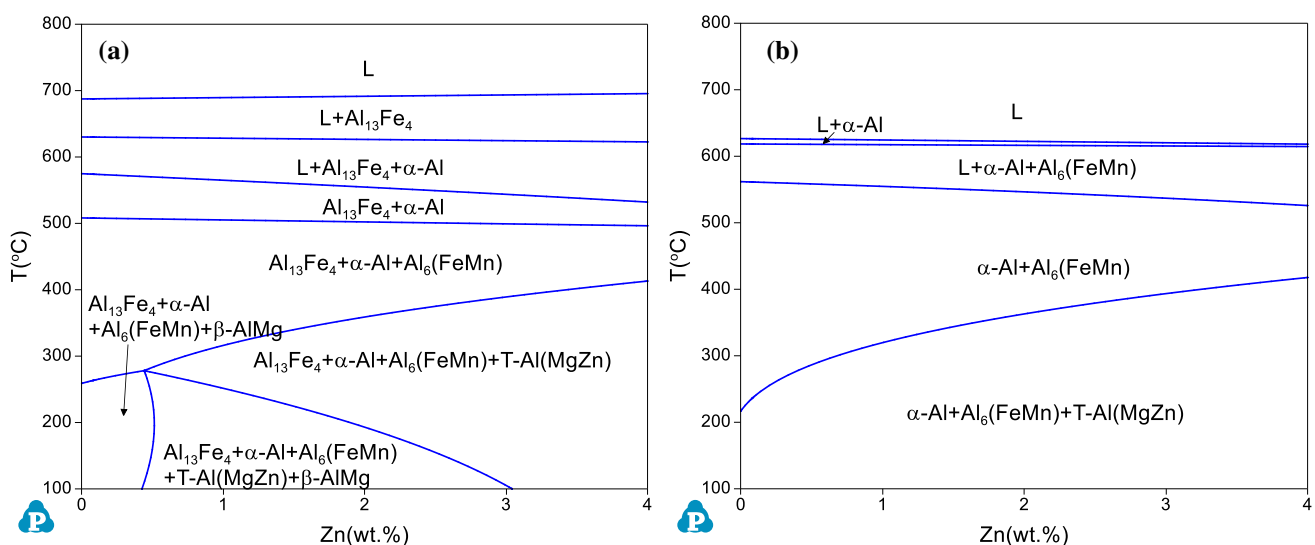


Figure 11 The **a** equilibrium and **b** metastable equilibrium phase diagram of Al–Mg–Fe–Mn–Zn system on the cross section of the Al–5Mg–1.5Fe–0.5Mn calculated using Pandat software.

critical role in suppressing the phase transformation from metastable $Al_6(Fe, Mn)$ phase to stable $Al_{13}Fe_4$ phase under non-equilibrium solidification conditions [18], leading to the existence of metastable $Al_6(Fe, Mn)$ phase as the dominant phase. The absence of $\beta-AlMg$ phase is also controlled by the high cooling rate during HPDC process, which dramatically lowers the diffusion of Mg atoms through $\alpha-Al$ matrix to $\alpha-Al$ grain boundary area and thus hinders the solid reaction for the formation of $\beta-AlMg$. It can be supported by the fact shown in Table 2 that abundant Mg atoms have been locked in $\alpha-Al$ phase as solute atoms. Furthermore, the formation of $T-Mg_{32}(Al, Zn)_{49}$ phase also depends on solid reaction and atomic diffusion through $\alpha-Al$ matrix and thus can be also suppressed by the high cooling rate. As the result, abundant solute Zn atoms are also detected in $\alpha-Al$ matrix as shown in Table 2. However, different with the completely disappeared $\beta-AlMg$ phase, the formation of $T-Mg_{32}(Al, Zn)_{49}$ phase has not been fully suppressed.

Considering the disappearance of $Al_6(Fe, Mn)$ and $\beta-AlMg$ phases in the as-cast alloys, a metastable equilibrium phase diagram was further calculated and is shown in Fig. 11b, and the phase fraction in the $AlMgFeMn$ alloys with different Zn levels is illustrated in Fig. 12. It is found that the increasing Zn level has almost no effect on the formation of $Al_6(Fe, Mn)$, but increases the amount and initial precipitation temperature of $T-Mg_{32}(Al, Zn)_{49}$ phase. But, the initial precipitation temperatures of

$T-Mg_{32}(Al, Zn)_{49}$ phase in all experimental alloys via solid–solid reaction are below 400 °C, indicating the low solution temperature (430 °C) is sufficient for the experimental alloys to dissolve the $T-Mg_{32}(Al, Zn)_{49}$ phase completely.

As mentioned above, although the Zn-containing stable phase in as-cast $Al-5Mg-1.5Fe-0.5Mn-3.09Zn$ alloy is $T-Mg_{32}(Al, Zn)_{49}$ phase, the precipitates in the aged alloy were identified as metastable η' phase in Fig. 10, rather than the corresponding precursors of $T-Mg_{32}(Al, Zn)_{49}$ phase (i.e. T' or T'' phase). The existing literature indicates that η' phase and its corresponding stable $\eta-MgZn_2$ phase are very common in $Al-Zn-Mg$ alloys [28, 29], while $T-Mg_{32}(Al, Zn)_{49}$ and its precursors (i.e. T' and T'' phases) are often observed in $Al-Mg-Zn$ alloys [5, 7, 8, 19, 20, 25, 26] [22, 23]. However, it was also reported that the precipitate in several cast $Al-Mg-Zn$ alloys with non-negligible Cu or Si levels, including $Al-10.2Mg-3.2Zn-2.7Si$ aged at 160 °C [30], $Al-8.1Mg-3.5Zn-2.6Si$ aged at 180 °C [10] and $Al-5Mg-3.09Zn-1.0Cu$ aged at 150 °C [21], is η' phase. It indicates that the phase transformation between η' and T' or T'' phases in $Al-Mg-Zn$ alloys maybe exists. As a reference, the phase transformation between η' and T -phase-based precipitates in $Al-Zn$ alloys has been confirmed, and one of the trigger factors is ageing temperature [29, 31]. As for the $Al-Mg-Zn$ alloys, the precise mechanism controlling the formation of these precipitates has not been revealed. However, by reviewing the above-mentioned studies

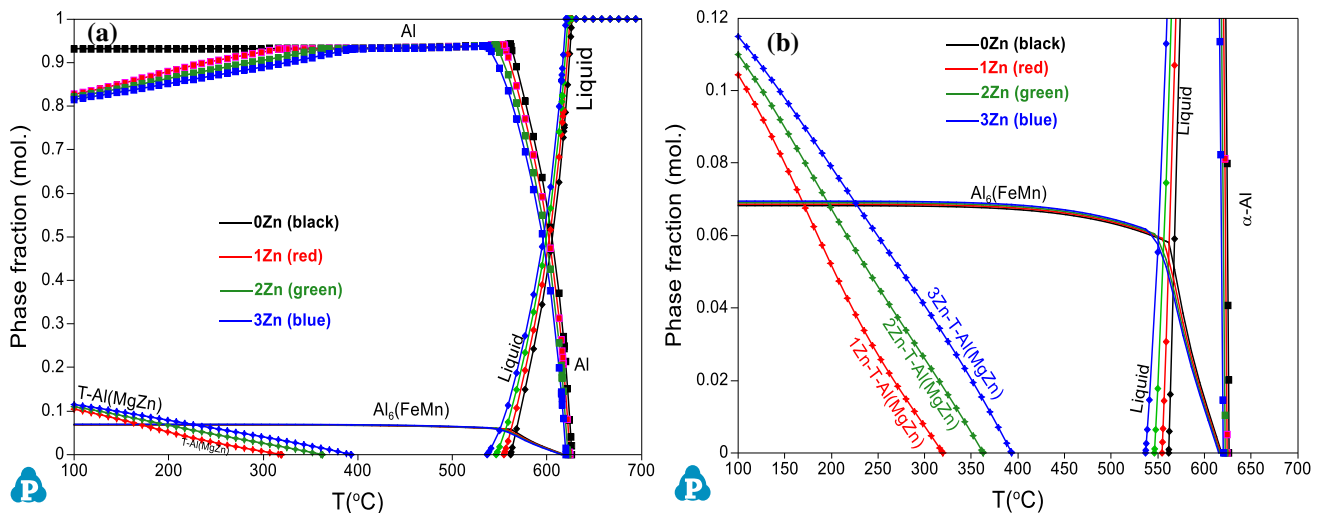


Figure 12 Phase fraction of the $Al-5Mg-1.5Fe-0.5Mn$ with different Zn levels calculated using Pandat software. **b** The enlarged part of (a).

[5, 7, 8, 10, 19–23, 25, 26, 30], we can speculate that some added elements (such as Cu and Si) may play a critical role in the formation of η' and T' or T'' precipitates. We also noticed that an HPDC Al–5Mg–0.8Mn–3.8Zn alloy (its composition except 1.5%Fe is very close to our studied Al–5Mg–1.5Fe–0.5Mn–3Zn alloy) aged at 120 °C is strengthened by T-phase-based precipitates (i.e. T' or T'') and cannot reach its peaking hardness even after a long ageing time 110 h [22, 23]. This phenomenon reminds us that the presence of Fe in high amounts (1.5 wt%) might be the reason for the observation of η' precipitate rather than T-phase-based precipitates (i.e. T' or T''). To verify this assumption and reveal the detailed mechanism, a systematic study is still needed.

Relationship between microstructure and mechanical properties

The mechanical properties of the experimental alloys are determined by their microstructures, including matrix and strengthening phases. To further understand the underlying mechanism of the mechanical properties variation in the experimental alloys, the fractured surfaces and cross sections of the as-cast and T6-treated alloys after tensile test at room temperature were analysed, and the results are exhibited in Figs. 13 and Fig. 14, respectively.

As shown in Fig. 13, the fractured surfaces of the as-cast and T6-treated alloys comprise many dimples and cracked $Al_6(Fe, Mn)$ particles. Among them, $Al_6(Fe, Mn)$ particles, especially the larger $Al_6(Fe, Mn)$ particles, show obvious cleavage facets and steps, which are the features of local brittle fracture. From Fig. 14, it can be found that almost all $Al_6(Fe, Mn)$ particles close to the fracture surfaces are cracked. Therefore, the fracture of strengthening $Al_6(Fe, Mn)$ phase is a main reason for the failure of experimental alloys. But, the variation in mechanical properties of the experimental alloys is decided by Zn addition. In as-cast alloy, the Zn additions form irregular $T-Mg_{32}(Al, Zn)_{49}$ phase at α -Al grain boundary and solute atoms within α -Al grains. The $T-Mg_{32}(Al, Zn)_{49}$ phase and solute Zn atoms can be the obstacles for the movement of dislocation and induce stress concentration, thus leading to the second phase strengthening effect and solid solution strengthening effect, respectively. But, the stress concentration around $T-Mg_{32}(Al, Zn)_{49}$ phase located at α -Al grain boundary also creates the crack at α -Al grain boundary area more easily. As shown in Fig. 14c, some cracks can be observed at the α -Al grain boundary and thus are also an important reason for the decreased ductility of the experimental alloys. After T6 heat treatment, the large $T-Mg_{32}(Al, Zn)_{49}$ phase is transformed to fine and well-distributed η' precipitates within α -Al grains and thus

Figure 13 SEM images showing fractured surface of AlMgFeMn alloys with **a**, **b** 0.02Zn and **c**, **d** 3.09Zn after tensile test: **a**, **c** as-cast, **b**, **d** T6-treated.

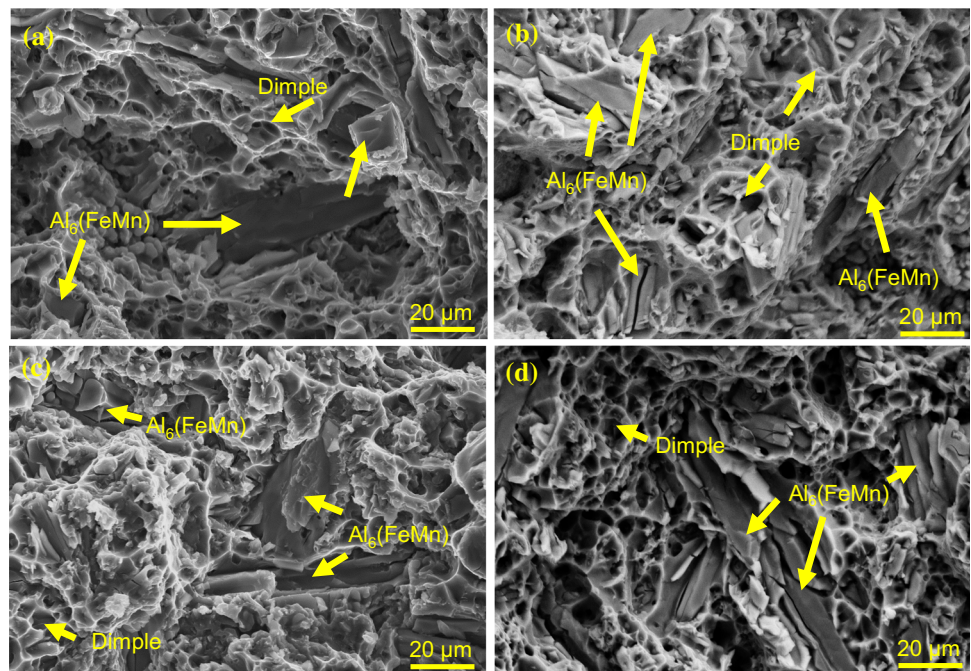
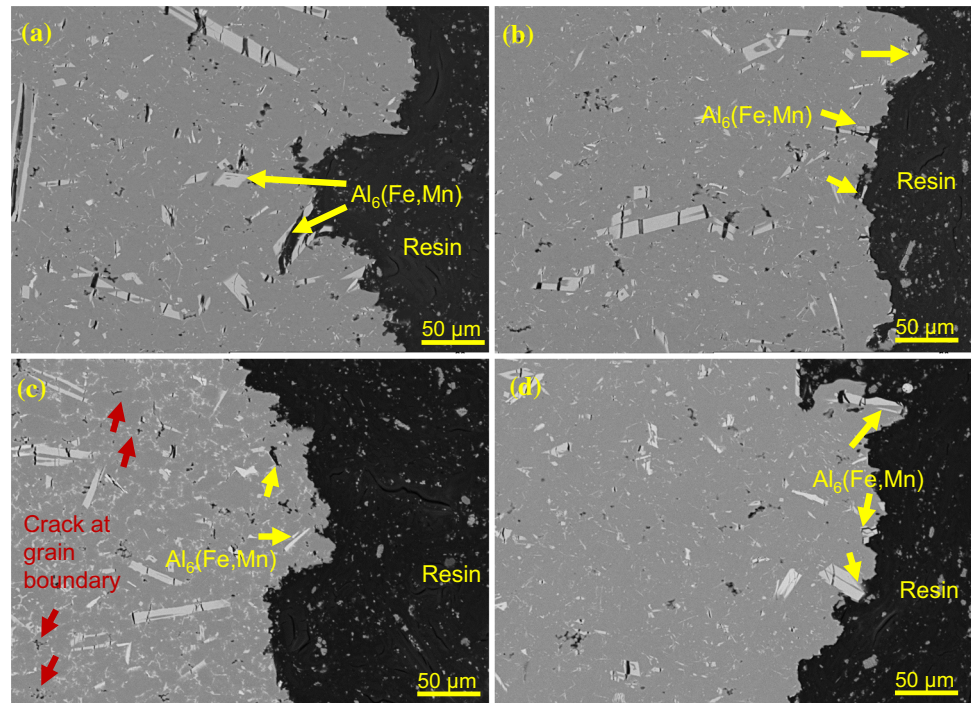


Figure 14 SEM images showing the cross sections of AlMgFeMn alloys with **a**, **b** 0.02Zn and **c**, **d** 3.09Zn after tensile test: **a**, **c** as-cast, **b**, **d** T6 treated.



provides a much better strengthening effect but at a less reduction in ductility. The dimples are considered as the feature of ductile fracture of alloys. From Fig. 13, it can be seen that the quantity of dimples becomes more but the sizes become smaller as the increment of Zn levels, indicating that the low Zn-containing alloys have more ductile behaviours compared to the high Zn-containing alloys. Therefore, T6 heat treatment can improve the ductility of the alloys, and these findings agree well with the results of tensile tests displayed in Figs. 5 and 9.

An inevitable problem of HPDC is the gas-containing porosity in the castings due to the high turbulence of melt flow during the die-filling process. At high temperatures such as during solution treatment, this compressed gas in porosities would expand largely and then result in surface blistering, reduction in mechanical property and the distortion of casting geometry. Therefore, heat treatment process is normally not preferred on HPDC castings. In recent years, Lumley [32, 33], Ji [6, 18, 28, 34] and Cecchel [34] confirmed that HPDC components can be successfully heat treated without causing significant surface blistering or distortion if the solution treatment is carried out at lower temperatures (e.g. 440 °C to 490 °C for Al–Si–Mg alloys) than normal temperatures. In this regard, the application of Zn in Al–Mg

alloys is significantly meaningful because of the effective solution at low temperature.

Conclusions

In the present paper, the effect of Zn level on the phase formation, microstructural evolution and mechanical properties of the Al–5Mg–1.5Fe–0.5Mn alloy processed by high-pressure die casting was investigated under as-cast and heat-treated conditions, and the main results were concluded as follows:

- (1) In the Al–5Mg–1.5Fe–0.5Mn alloy, the addition of Zn increases the phase fraction of T-Mg₃₂(Al, Zn)₄₉ but has no significant effect on the formation of Al₆(Fe, Mn) and α-Al phases in as-cast microstructure.
- (2) T-Mg₃₂(Al, Zn)₄₉ phase in the as-cast microstructure can be completely dissolved into the α-Al matrix after the solution at a relative lower temperature 430 °C, and fine η' precipitates are formed during the subsequent ageing at 120 °C.
- (3) The addition of Zn makes the experimental Al–5Mg–1.5Fe–0.5Mn alloy heat-treatable and can increase the tensile strength under both as-cast and T6-treated conditions with the sacrifice of

ductility. The as-cast alloy with 3.09Zn offers the ultimate tensile strength of 335 MPa, yield strength of 239 MPa and elongation of 3.7%. After the optimized T6 heat treatment (solution at 430 °C for 60 min and ageing at 120 °C for 16 h), the ultimate tensile strength, yield strength and elongation are further significantly increased to 445 MPa, 321 MPa and 6.2%, respectively.

Acknowledgements

Financial support from Innovate UK under Project 11019 is gratefully acknowledged.

Authors contribution

Xiangzhen Zhu and Fuchu Liu contributed equally to this work.

Declaration

Conflict of interest The authors declare that they have no conflict of interest.

Open Access This article is licensed under a Creative Commons Attribution 4.0 International License, which permits use, sharing, adaptation, distribution and reproduction in any medium or format, as long as you give appropriate credit to the original author(s) and the source, provide a link to the Creative Commons licence, and indicate if changes were made. The images or other third party material in this article are included in the article's Creative Commons licence, unless indicated otherwise in a credit line to the material. If material is not included in the article's Creative Commons licence and your intended use is not permitted by statutory regulation or exceeds the permitted use, you will need to obtain permission directly from the copyright holder. To view a copy of this licence, visit <http://creativecommons.org/licenses/by/4.0/>.

References

- [1] Zolotarevsky VS, Belov NA, Glazoff MV (2007) Casting aluminum alloys, 1 edn. Elsevier Ltd, Amsterdam. <https://doi.org/10.1016/B978-0-08-045370-5.X5001-9>
- [2] Yang H, Watson D, Wang Y, Ji S (2014) Effect of nickel on the microstructure and mechanical property of die-cast Al–Mg–Si–Mn alloy. *J Mater Sci* 49:8412–8422. <https://doi.org/10.1007/s10853-014-8551-2>
- [3] Ji S, Watson D, Fan Z, White M (2012) Development of a super ductile diecast Al–Mg–Si alloy. *Mater Sci Eng A* 556:824–833
- [4] Zhang X, Chen Y, Hu J (2018) Recent advances in the development of aerospace materials. *Prog Aerosp Sci* 97:22–34
- [5] Meng C, Zhang D, Cui H, Zhuang L, Zhang J (2014) Mechanical properties, intergranular corrosion behavior and microstructure of Zn modified Al–Mg alloys. *J Alloy Compd* 617:925–932
- [6] Yang X, Chen J, Liu J, Qin F, Xie J, Wu C (2014) A high-strength AlZnMg alloy hardened by the T-phase precipitates. *J Alloy Compd* 610:69–73
- [7] Hou S, Liu P, Zhang D, Zhang J, Zhuang L (2018) Precipitation hardening behavior and microstructure evolution of Al–5.1Mg–0.15Cu alloy with 3.0Zn (wt%) addition. *J Mater Sci* 53:3846–3861. <https://doi.org/10.1007/s10853-017-1811-1>
- [8] Hou S, Zhang D, Ding Q, Zhang J, Zhuang L (2019) Solute clustering and precipitation of Al–5.1Mg–0.15 Cu–xZn alloy. *Mater Sci Eng A* 759:465–478
- [9] Ji S, Yan F, Fan Z (2015) Development of a high strength Al–Mg₂Si–Mg–Zn based alloy for high pressure die casting. *Mater Sci Eng A* 626:165–174
- [10] Li L, Ji S, Zhu Q, Wang Y, Dong X, Yang W, Midson S, Kang Y (2018) Effect of Zn concentration on the microstructure and mechanical properties of Al–Mg–Si–Zn alloys processed by gravity die casting. *Metall Mater Trans A* 49:3247–3256
- [11] Trudonoshyn O, Rehm S, Randelzhofer P, Körner C (2019) Improvement of the high-pressure die casting alloy Al–5.7Mg–2.6Si–0.7Mn with Zn addition. *Mater Charact* 158:109959
- [12] Guo M, Zhang Y, Zhang X, Zhang J, Zhuang L (2016) Non-isothermal precipitation behaviors of Al–Mg–Si–Cu alloys with different Zn levels. *Mater Sci Eng A* 669:20–32
- [13] Guo M, Du J, Zheng C, Zhang J, Zhuang L (2019) Influence of Zn levels on precipitation and corrosion of Al–Mg–Si–Cu–Zn alloys for automotive applications. *J Alloy Compd* 778:256–270
- [14] Yuan B, Guo M, Wu Y, Zhang J, Zhuang L, Lavernia EJ (2019) Influence of treatment pathways on the precipitation behaviors of Al–Mg–Si–Cu–(Zn)–Mn alloys. *J Alloy Compd* 797:26–38
- [15] Dong X, Zhu X, Ji S (2019) Effect of super vacuum assisted high pressure die casting on the repeatability of mechanical

- properties of Al–Si–Mg–Mn die-cast alloys. *J Mater Process Technol* 266:105–113
- [16] Zhu X, Dong X, Blake P, Ji S (2020) Improvement in as-cast strength of high pressure die-cast Al–Si–Cu–Mg alloys by synergistic effect of η -Al₃Cu₂Mg₈Si₆ and θ -Al₂Cu phases. *Mater Sci Eng A* 802:140612
- [17] Zhu X, Blake P, Dou K, Ji S (2018) Strengthening die-cast Al–Mg and Al–Mg–Mn alloys with Fe as a beneficial element. *Mater Sci Eng A* 732:240–250
- [18] Zhu X, Blake P, Ji S (2018) The formation mechanism of Al₆(Fe, Mn) in die-cast Al–Mg alloys. *CrystEngComm* 20:3839–3848
- [19] Meng C, Zhang D, Zhuang L, Zhang J (2016) Correlations between stress corrosion cracking, grain boundary precipitates and Zn level of Al–Mg–Zn alloys. *J Alloy Compd* 655:178–187
- [20] Ding Q, Zhang D, Pan Y, Hou S, Zhuang L, Zhang J (2019) Strengthening mechanism of age-hardenable Al–xMg–3Zn alloys. *Mater Sci Technol* 35:1071–1080
- [21] Tang HP, Wang QD, Lei C, Ye B, Wang K, Jiang HY, Ding WJ, Zhang XF, Lin Z, Zhang JB (2019) Effect of cooling rate on microstructure and mechanical properties of an Al–5.0Mg–3.0Zn–1.0Cu cast alloy. *J Alloys Comps* 801:596–608
- [22] Stemper L, Tunes MA, Oberhauser P, Uggowitzer PJ, Pogatscher S (2020) Age-hardening response of AlMgZn alloys with Cu and Ag additions. *Acta Materialia* 195:541–554
- [23] Stemper L, Mitas B, Kremmer T, Otterbach S, Uggowitzer PJ, Pogatscher S (2019) Age-hardening of high pressure die casting AlMg alloys with Zn and combined Zn and Cu additions. *Mater Des* 181:107927
- [24] Ji S, Yang W, Gao F, Watson D, Fan Z (2013) Effect of iron on the microstructure and mechanical property of Al–Mg–Si–Mn and Al–Mg–Si diecast alloys. *Mater Sci Eng A* 564:130–139
- [25] Cao C, Zhang D, He Z, Zhuang L, Zhang J (2016) Enhanced and accelerated age hardening response of Al–5.2Mg–0.45Cu (wt%) alloy with Zn addition. *Mater Sci Eng A* 666:34–42
- [26] Cao C, Zhang D, Wang X, Ma Q, Zhuang L, Zhang J (2016) Effects of Cu addition on the precipitation hardening response and intergranular corrosion of Al–5.2Mg–2.0Zn (wt%) alloy. *Mater Charact* 122:177–182
- [27] Kverneland A, Hansen V, Thorkildsen G, Larsen H, Pattison P, Li X, Gjønnes J (2011) Transformations and structures in the Al–Zn–Mg alloy system: a diffraction study using synchrotron radiation and electron precession. *Mater Sci Eng A* 528:880–887
- [28] Yang W, Ji S, Wang M, Li Z (2014) Precipitation behaviour of Al–Zn–Mg–Cu alloy and diffraction analysis from η' precipitates in four variants. *J Alloy Compd* 610:623–629
- [29] Löffler H, Kovacs I, Lendvai J (1983) Decomposition processes in Al–Zn–Mg alloys. *J Mater Sci* 18:2215–2240. <https://doi.org/10.1007/BF00541825>
- [30] Yang W, Liu L, Zhang J, Ji S (2017) Insight into the partial solutionisation of a high pressure die-cast Al–Mg–Zn–Si alloy for mechanical property enhancement. *Mater Sci Eng A* 682:85–89
- [31] Vlach M, Cizek J, Kodetova V, Leibner M, Cieslar M, Harcuba P, Bajtosova L, Kudrnova H, Vlasak T, Neubert V (2020) Phase transformations in novel hot-deformed Al–Zn–Mg–Cu–Si–Mn–Fe (–Sc–Zr) alloys. *Mater Des* 193:108821
- [32] Lumley RN, Polmear I, Curtis P (2009) Rapid heat treatment of aluminum high-pressure diecastings. *Metall Mater Trans A* 40:1716–1726
- [33] Lumley R (2011) Progress on the heat treatment of high pressure die castings. In: *Fundamentals of aluminium metallurgy*. Elsevier, pp 262–303
- [34] Cecchel S, Panvini A, Cornacchia G (2018) Low solution temperature heat treatment of AlSi 9Cu3 (Fe) high-pressure die-casting actual automotive components. *J Mater Eng Perform* 27:3791–3802

Publisher's Note Springer Nature remains neutral with regard to jurisdictional claims in published maps and institutional affiliations.